Accurate optical flow field estimation using mechanical properties of soft tissues

Hatef Mehrabian[*a], Hirad Karimi[a], Abbas Samani[a,b,c]

[a]Department of Electrical & Computer Engineering, University of Western Ontario, London, ON, Canada
[b]Department of Medical Biophysics, University of Western Ontario, London, ON, Canada
[c]Imaging Research Laboratories, Robarts Research Institute, London, ON, Canada

ABSTRACT

A novel optical flow based technique is presented in this paper to measure the nodal displacements of soft tissue undergoing large deformations. In hyperelasticity imaging, soft tissues maybe compressed extensively [1] and the deformation may exceed the number of pixels ordinary optical flow approaches can detect. Furthermore in most biomedical applications there is a large amount of image information that represent the geometry of the tissue and the number of tissue types present in the organ of interest. Such information is often ignored in applications such as image registration. In this work we incorporate the information pertaining to soft tissue mechanical behavior (Neo-Hookean hyperelastic model is used here) in addition to the tissue geometry before compression into a hierarchical Horn-Schunck optical flow method to overcome this large deformation detection weakness. Applying the proposed method to a phantom using several compression levels proved that it yields reasonably accurate displacement fields. Estimated displacement results of this phantom study obtained for displacement fields of 85 pixels/frame and 127 pixels/frame are reported and discussed in this paper.

Keywords: Image registration, Hyperelasticity, Modeling, Optical flow, Hierarchical, Horn_Schunck

1. INTRODUCTION

Estimating optical flow is an important problem in computer vision. Optical flow is the apparent motion between two frames in an image sequence [2]. This motion is determined based on the main features of the image i.e., intensity variations, points, lines, etc.[3]. In computer vision the primary emphasis is on determining instantaneous image velocities [4-6] and displacements of points between successive image frames [7-8]. There also exist some methods that attempt to track lines and curves [9,10]. Optical flow estimation is based on the assumption that objects in the image sequence change position and deform but their appearance remains constant. This is called the brightness constancy assumption. This assumption by itself leads to an under-determined system of equations for determining the point displacements, therefore other assumptions are needed. Various methods have proposed different assumptions that can be divided into global and local assumptions. Horn and Schunck 1981 [5] added a smoothness term to regularize the flow which is a local assumption. With medical images, we commonly view opaque objects of finite size undergoing rigid motion or deformation. In such cases, smoothness of velocity field is an appropriate assumption. Lucas and Kanade [11] proposed another method where they assumed constant motion in a small window. This approach leads to a local least squares calculation.

Elastography is a non-invasive imaging technique that uses tissue stiffness as a contrast mechanism for tissue abnormality detection and disease diagnosis. In hyperelastic elastography [1] the tissue is mechanically stimulated with large deformation. This is followed by reconstructing the tissues' hyperelastic parameters using tissue displacement data. The reconstructed hyperelastic parameters have the potential to be used for cancer detection and diagnosis. Such parameters can also be used as input parameters in tissue biomechanical models developed to estimate tissue

*hmehrabi@uwo.ca; phone 1 416 826-3273;

Medical Imaging 2009: Biomedical Applications in Molecular, Structural, and Functional Imaging, edited by Xiaoping P. Hu, Anne V. Clough, Proc. of SPIE Vol. 7262, 72621B · © 2009 SPIE · CCC code: 1605-7422/09/$18 · doi: 10.1117/12.813897

displacements. Estimating tissue deformation has great significance in several medical applications such as surgery or brachethrapy planning and guidance [12]. To perform hyperelastic elastography, accurate acquisition of tissue displacements as it undergoes deformation, is a crucial step to ensure reliable parameter reconstruction [1].

Optical flow field estimation using conventional algorithms aims at obtaining small velocity fields via computation of spatial and temporal image derivatives. In such algorithms, detailed and piecewise variations are handled efficiently using partial derivatives. Applying conventional optical flow algorithms where large motion is involved yields ill-posed systems leading to local minima corresponding to inappropriate matching [13]. To overcome these issues, hierarchical algorithms have been proposed based on multi-resolution representation [3-14]. Although these optical flow methods are designed to measure displacement fields for the so called large deformations, their compression level is still small for what is needed in nonlinear elastography. The level of compression required for elastography is so high (about 100 pixels/frame) and these methods cannot track such high tissue motion with enough accuracy. To our knowledge, there is no optical flow based algorithm capable of estimating large tissue displacements involved in hyperelastic elastography. In this study we propose a novel displacement tracking technique for large deformation based on a hierarchical Horn-Schunck optical flow method. Hereby, we use the initial geometry of the tissue and its mechanical properties to improve the accuracy of displacement measurement.

The organization of this paper is as follows. First a brief description of the optical flow method used here is given. Next, the hierarchical optical flow approach is described. This is followed by introducing the proposed algorithm in the Methods section. A byproduct of the proposed technique is estimating values of the tissue hyperelastic parameters. In this article we will introduce the governing equation of tissue stress-deformation and its use for reconstructing the mechanical properties of the tissues.

2. THEORY

The novel displacement data acquisition method presented here incorporates information of the soft tissue mechanical properties into the hierarchical Horn-Schunck optical flow algorithm in order to determine displacement field corresponding to large deformation involved in medical applications. This will be described in details in the Methods after presenting the Horn-Schunck optical flow techniques.

2.1. Horn-Schunck optical flow method

The basic Horn-Schunck algorithm is a differential based optical flow method suitable for applications where small displacements are involved. These methods compute velocity from spatiotemporal derivatives of image intensity or filtered versions of the image. The fundamental assumption of all conventional optical flow methods is the brightness constancy given in equation (1):

$$I(x,t) \approx I(x+\delta x, t+\delta t) \tag{1}$$

where I is the intensity value of a pixel located at position x at time t. Brightness constancy equation (BCE) assumes that the brightness pattern of the object between two consecutive frames is constant. Equation (1) is also expressed as the following equation, which is known as the optical flow constraint equation,

$$\frac{dI(u,v,t)}{dt} = \frac{\partial I}{\partial u}\frac{\partial u}{\partial t} + \frac{\partial I}{\partial v}\frac{\partial v}{\partial t} + \frac{\partial I}{\partial t} = 0 \qquad or \qquad \nabla I \cdot v + I_t = 0 \tag{2}$$

where v is the velocity vector. Constraints are required because the velocity field at each image point has two components while the change in image brightness at a point in the image plane due to motion yields only one equation. Using this equation alone yields an under-determined system of equations, which cannot be solved without adding further constraints. Horn and Schunck combined brightness constancy constraint with a global smoothness term to constrain the estimated velocity field. This is done by minimizing the error functional which combines the brightness constancy and smoothness constraint over the image domain D and yields the following equation:

$$\int_D \left(\nabla I.v + I_t\right)^2 + \lambda^2 \left(\|\nabla u\|_2^2 + \|\nabla v\|_2^2\right) dx \tag{3}$$

where ||.||2 denotes the L2 norm and the magnitude of λ reflects the influence of the smoothness term. This additional constraint is an appropriate constraint especially with applications involving tissue deformation estimation. The above equation is solved for velocity vector by iterating over Gauss-Seidel equations given as follows:

$$u^{k+1} = \bar{u}^{k} - \frac{I_x\left[I_x\bar{u}^{k} + I_y\bar{v}^{k} + I_t\right]}{\alpha^2 + I_x^2 + I_y^2} \qquad \& \qquad v^{k+1} \equiv \bar{v}^{k} - \frac{I_y\left[I_x\bar{u}^{k} + I_y\bar{v}^{k} + I_t\right]}{\alpha^2 + I_x^2 + I_y^2} \tag{4}$$

where k denotes the iteration number, u^0 and v^0 denote the initial velocity estimates and $\bar{u}^k$ and $\bar{v}^k$ denote the neighborhood averages of u^k and v^k. Also, I_x, I_y and I_t are the derivatives of image intensity function I with respect to x, y and t, respectively. In order to have a good optical flow estimation, we need to provide sufficiently accurate approximation of derivatives of image intensity function. For this purpose, we preprocessed the images by applying a Gaussian pre-filter with a standard deviation of 1.5 pixels in space and 1.5 frames in time (1.5 pixel-frames). Furthermore, we used λ = 0.5 instead of the λ= 100 suggested by Horn and Schunck 1981 [5] which turned out to produce better results in our application.

The original method of Horn & Schunck 1981 [5] uses 2 images only to estimate intensity derivatives I_x , I_y and I_t . In the hierarchical pyramid optical flow described in the next section, these derivatives are calculated in each step of the Gaussian pyramid using the following masks:

$$M_x = \frac{1}{4}\begin{pmatrix} -1 & 1 \\ -1 & 1 \end{pmatrix} \quad , \quad M_y = \frac{1}{4}\begin{pmatrix} 1 & 1 \\ -1 & -1 \end{pmatrix} \quad , \quad M_t = \frac{1}{4}\begin{pmatrix} 1 & 1 \\ 1 & 1 \end{pmatrix} \tag{5}$$

where M_x , M_y and M_t are convolution kernels along x, y and t directions, respectively. The neighborhood average is calculated using Equation (6):

$$M_H = \begin{pmatrix} \frac{1}{12} & \frac{1}{6} & \frac{1}{12} \\ \frac{1}{6} & 0 & \frac{1}{6} \\ \frac{1}{12} & \frac{1}{6} & \frac{1}{12} \end{pmatrix}$$

$$\bar{u}^k = u^k * M_H \tag{6}$$

$$\bar{v}^k = v^k * M_H$$

In applications where tissue deformation is involved, displacement smoothness should be taken into account. This constraint is applicable to both small and large tissue deformation. The method requires iterative solution for equation (4). The number of iterations is typically hundreds (200 iteration are used in this study), which renders the methods computationally expensive.

2.2. Hierarchical Pyramid optical flow Method

The Horn-Schunck optical flow method is not suitable for determining the displacement field in applications where large deformation is involved. Hierarchical pyramid approach is proposed to address this weakness. Multi-resolution representations of an image are called image pyramids. The coarser images are blurred and sub-sampled showing the gross image motion while the fine deformations of the image are shown in the high resolution images. Level 0 is the original image, the image in each level is constructed by blurring the image in the previous level with a 2D separable Gaussian filter (with standard deviation of 1) and then sub-sampling the resultant image by a factor of 2 in the image dimensions. A four level pyramid is used in this study having resolutions of 1, 1/2, 1/4 and 1/8 of the original image. In the hierarchical coarse to fine pyramid technique used here, the velocity field is calculated at the top of the pyramid [15].

Once the sub-sampled images are constructed, the velocity vectors are calculated for each pair of images in the pyramid. Using more efficient differentiation kernels than simple pixel differences was crucial to obtaining good optical flow estimates. Therefore, for each pair of images, we applied pre-smoothing Gaussian filter with 1.5 pixel-frame followed by using the differentiation kernels of equation (5).

Images are then warped based on the calculated velocity vectors. The image velocity parametric model (Horn-Schunck) introduced in the previous section is sufficiently accurate for small motions; however, for cases involving large motions, images have to be warped before they are processed. Image warping is performed by using a computed flow field as the initial velocities at each pixel (x, y) in the sequence. For pixel location (x, y) where i and j are the integer values of x and y, respectively. Assuming I_1 , I_2, I_3 and I_4 are the brightness at points (i, j), $(i + 1, j)$, $(i + 1, j + 1)$ and $(i, j + 1)$, respectively, the intensity of pixel (x,y) can be computed as follows:

$$I(x, y) = (1 - u)(1 - v)I_1 + uI_2 + v(1 - u)I_4 + uI_3 \tag{8}$$

This process must be repeated until we reach the bottom of the pyramid where level 0 images are located. Hierarchical framework for calculating optical flow is illustrated in Fig. 1.

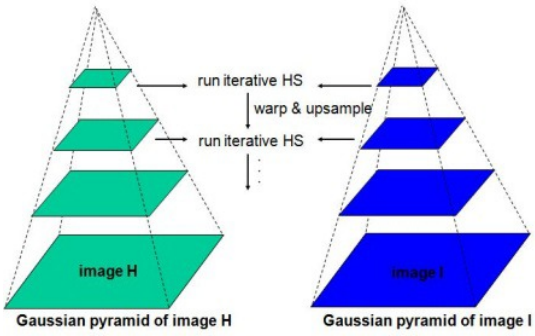

Fig. 1: Hierarchical framework for optical flow computation

2.3. Hyperelasticity

Our novel optical flow technique involves a non-linear finite element (FE) model of the imaged tissue. The tissue geometry before deformation is assumed to be known based on which the FE model is constructed. Our study involves a numerical 2D phantom that is composed of three different materials, representing a slice of cancerous breast that has three tissue types (adipose, fibroglandular tissue and tumor tissue).

The tissues are assumed hyperelastic which undergo large deformation. The constitutive model of the hyperelastic tissues are represented by a strain energy function. These functions are characterized by a number of coefficients called hyperelastic parameters. In this study we used Neo-Hookean strain energy function given in Equation (9).

$$U = C_{10}(I_1 - 3), \tag{9}$$

where C10 represents the hyperelastic parameter of this model. C10 is also known as the shear modulus of the tissue and I1 is the first strain invariant.

3. METHODS

The optical flow field computation process involves calculating initial optical flow field between the deformed image and the undeformed (baseline) image. This field is used to calculate the initial amount of compression applied to the phantom. Using an initial guess for the hyperelastic parameters of each tissue type, ABAQUS (commercial finite element solver) is employed for stress calculation. This stress field and the deformation field calculated using the optical flow algorithm are fed to an iterative optimization routine to determine the displacement field and the hyperelastic properties of the tissues. The flowchart of this method is illustrated in Fig. 2.

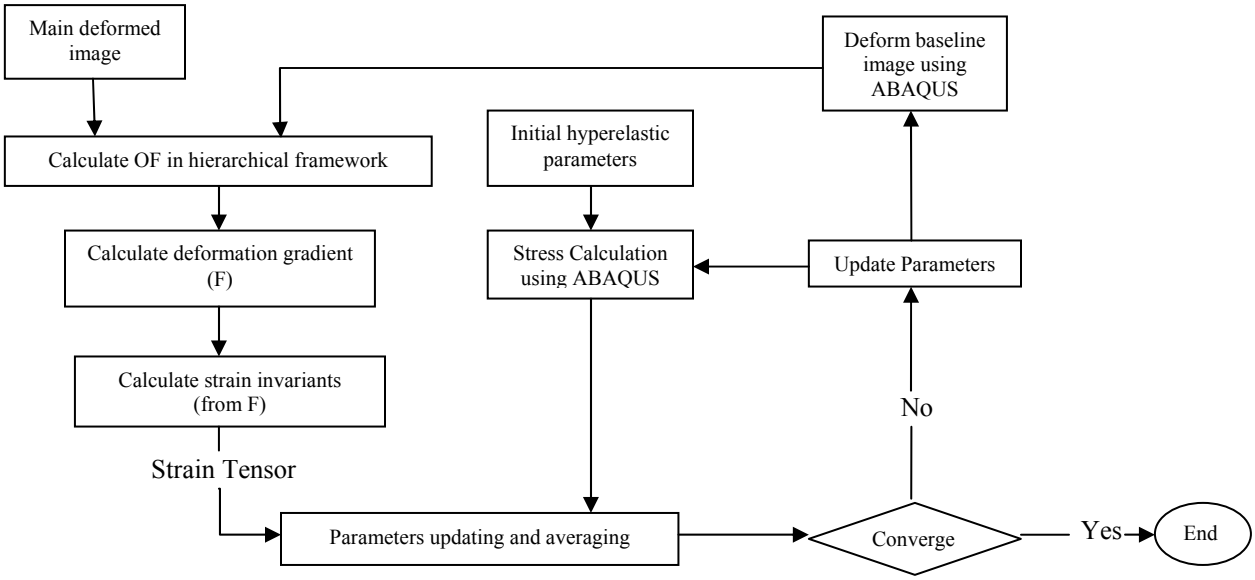

Fig. 2: Flowchart of proposed iterative optical flow field estimation

3.1. Deformation field estimation algorithm

The deformation field estimation process starts with applying the hierarchical optical flow technique to the baseline image (the image before deformation) and the deformed image. Once this initial rough estimate of the field is calculated an initial value is of compression level is also extracted from this data for the compression level applied to the tissue. The information about the compression level and the calculated initial deformation field along with an initial guess for the hyperelastic parameters of all three tissue types and the geometry information are fed to an iterative parameter reconstruction algorithm that is presented in [1] and is described in the next section.

Once the parameter reconstruction algorithm converges to its optimal parameters, the tissue deformation field acquired from ABAQUS simulation using these parameters and the calculated compression level are used to warp the baseline image to a new updated image called the updated baseline image. This updated baseline image, though being very different from the deformed image, is a rough estimate of the deformed image and has higher similarity level to the deformed image compared to the similarity between the baseline image and the deformed image. Next, the updated baseline image is used as the baseline image in the next iteration and the same procedure is followed until convergence is achieved. Convergence criterion to stop iterations is reaching small variations in the amount of compression level. The convergence criterion is small variation in the value of the reconstructed hyperelastic parameter. It works in conjunction with the criterion for stopping iteration of the parameter reconstruction algorithm.

We used normalized mutual information (NMI) similarity measure to calculate the similarity of two images in this study. Central to MI (mutual information) is the theory of Shannon entropy (Shannon 1948 [16]). By characterizing two images using the probability distribution function (PDF) based on the joint histogram of the two images and taking into account that minimizing the joint entropy correlates with better image-to-image alignment, a powerful image similarity measure is defined and called the normalized mutual information of the two images [17].

3.2. Iterative parameter reconstruction algorithm

The optimization routine uses the constitutive equation for stress-deformation that is given in equation (10)

$$\sigma = \frac{2}{J} DEV \left[\left(\frac{\partial U}{\partial \overline{I}_1} + \overline{I}_1 \frac{\partial U}{\partial \overline{I}_2} \right) \overline{B} - \frac{\partial U}{\partial \overline{I}_2} \overline{B}.\overline{B} \right] - pI \,, \tag{10}$$

where DEV represents the deviatoric part of the stress tensor, p is hydrostatic pressure and I is the identity matrix. $B = F^T.F$ where F is the deformation gradient and I_1, I_2 and J are the first, second and third strain invariants, respectively. For each element this equation is rearranged in the following form:

$$\{\sigma\} = [A]\{C\} \tag{11}$$

Where $\{\sigma\}$ is the element stress tensor, $[A]$ is the coefficient matrix formed using nodal displacements, and $\{C\}$ is the unknown hyperelastic parameters. Using Equation (11), the value of C10 is calculated using a least squares method. This yields a new hyperelastic parameter for each element in the mesh. Averaging these values over the volume of each tissue results in an updated tissue parameter. This iterative process continues until the value of C_{10} shows small variation, which means it has converged to its optimum value.

4. NUMERICAL PHANTOM STUDY

To simplify the analysis without loss of generality we assume to have a rectangular slice of breast tissue. We also assume to have a circular tumor in the center of the slice. The objective of this work is to perform optical flow field estimation on a 2D slice of a tissue. Thus we selected the simple geometry shown in Fig. 3 to validate the performance of the method. The method is independent of the shape of tissue and any other geometry can be used instead.

The selected geometry for the numerical phantom is rectangular which consists of three types of material corresponding to fibroglandular, adipose and cancerous tissues. We also placed a mesh on the tissue slice to compensate for the lack of intensity variations required for optical flow field estimation. Similar to the choice of the geometry, the intensity variations can be arbitrary and are not specific to the one used in this study. The mesh represents the biological landmarks existing in a breast tissue slice. Since the tissue is constructed numerically, we had to add some landmarks to compensate for this lack of information. This phantom is illustrated in Fig.3.

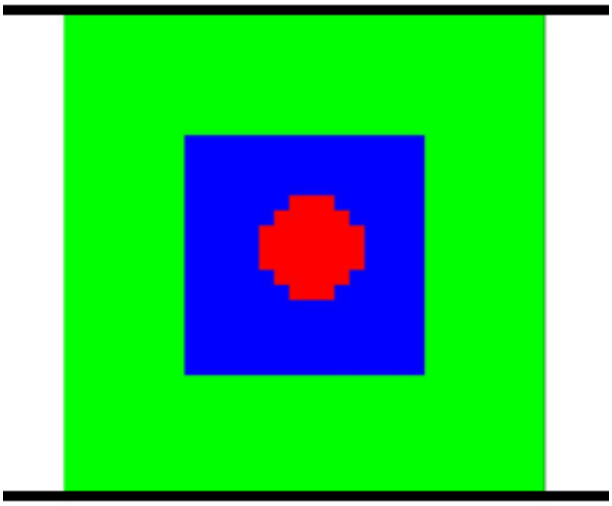

Fig. 3: Geometry of the numerical phantom used for validation, which consists of three different tissue types. The dots placed on the phantom are used for simulating intensity variations existing in a real tissue image. The top and bottom blades show the moving and fixed blades used for applying compression to the tissue.

The mechanical specifications (hyperelastic parameters) of each tissue type are calculated based on the measurements performed by Samani *et al* [18]. They reported the hyperelastic parameters of breast tissues for Polynomial strain energy unction. The corresponding Neo-Hookean parameters are calculated by fitting the stress-strain curves of the two hyperelastic models. The geometry and specifications of the undeformed image are fed to ABAQUS finite element solver to simulate its deformations under specific loadings. Displacement boundary condition is used for the top nodes and zero displacement is used at the bottom. The loading is quasi-static and is applied to the phantom in 10 steps. The deformed image for each of the two case studies is constructed by applying its specific amount of loading to the model using ABAQUS and extracting the deformations of the phantom. These deformations and the baseline image are used to

construct the deformed image. The constructed deformed images of the two cases (85 pixel/frame and 127 pixel/frame compressions) are depicted in Fig. 4a and Fig. 4b, respectively.

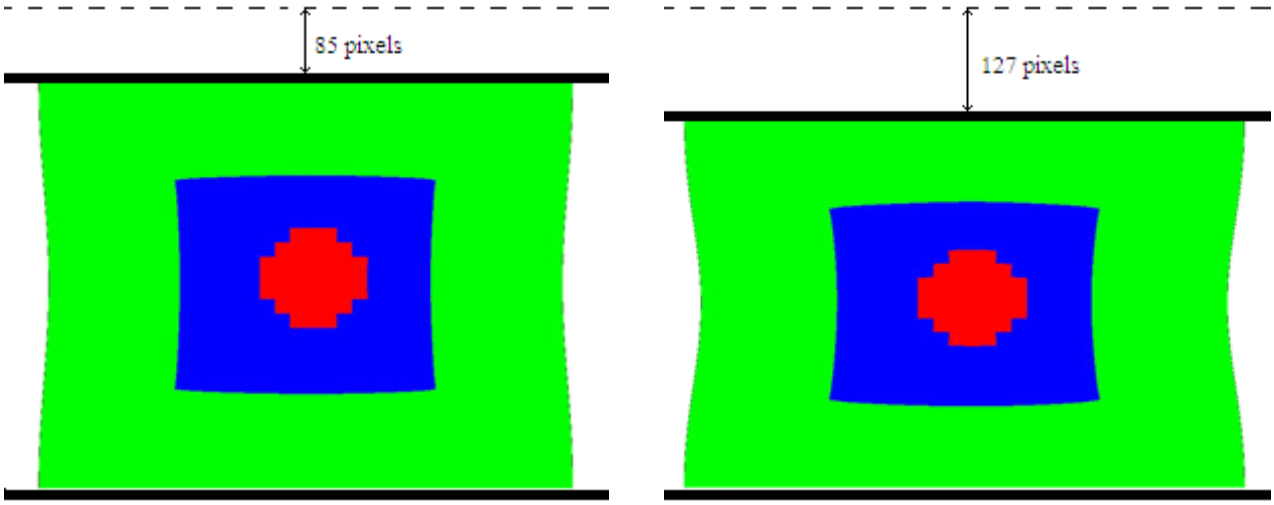

(a) (b)

Fig. 4: The numerically constructed deformed images for a) 85 pixel per frame compression and b) 127 pixel per frame compression. The initial state of the compression blade is shown by dashed line and it's final state is shown by thick solid line.

In each case study, the corresponding deformed image and the baseline undeformed images are fed to the hierarchical optical flow routine to calculate the initial estimate of the deformation field.

5. RESULTS

The proposed displacement field acquisition algorithm was tested on numerical phantom case studies involving several compression levels. The results obtained from these tests are promising. Here we report the results relating to the two highest compression levels we performed in our study. The first analysis corresponds to 85 pixels per frame displacement while the second corresponds to 127 pixels per frame. The compression levels given here are the maximum displacement of the phantom and correspond to its top nodes. Fig. 5a and b show the convergence of the compression level to its actual value (the compression used for constructing the deformed image) respectively. The convergence criterion used to stop the iterative process was the reaching a point in which we have negligible variations in the value of compression level in conjunction with having close to zero variation in the updated hyperelastic parameter value .

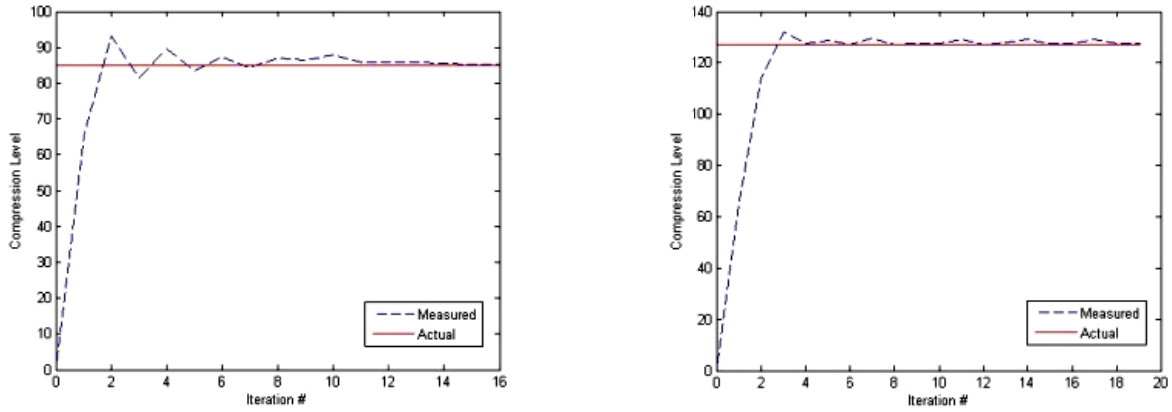

(a) (b)

Fig. 5: Convergence of the compression level to its actual value for a) 85 pixels per frame compression and b) 127 pixels per frame compression

Fig. 6a and b illustrate the normalized mutual information of the two deformed images and the numerically updated baseline image. These curves show the similarity between the updated baseline image and the deformed image. Both curves approach the maximum value of NMI which is equal to 2 and the ultimate similarity level reached for both cases show the high degree of similarity between the two images showing the good performance of the method.

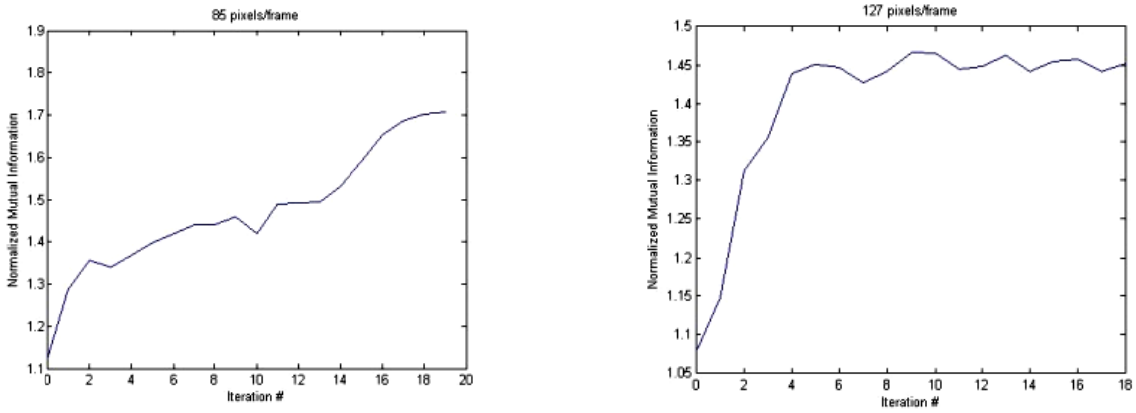

(a) (b)

Fig. 6: Normalized Mutual information value for a) 85 pixels per frame compression and b) 127 pixels per frame compression

Table 1 provides the value of NMI at the convergence point, the mean error of the displacements and the value and error of the compression level applied to the baseline image for both 85-pixel and 127-pixel compression levels and the number of iteration to achieve convergence.

Table. 1. The mean error of the displacements, the value and error of the compression level applied to the baseline image, the value of NMI at the convergence point and the number of iterations required for convergence

Compression level	Mean error of displacement (%)	Reconstructed compression level	Reconstructed compression level error (%)	Normalized Mutual Information value	Number of iterations
85 pixels/frame	5.0045%	85.349	0.4114	1.7059 (out of 2)	19
127 pixels/frame	5.3848%	127.675	0.5312	1.5575 (out of 2)	23

In Fig. 7 the baseline image, the deformed image, final numerically deformed image resulting from applying the proposed method, difference between the experimentally deformed and the numerically deformed images, the actual displacement field and the field acquired by the proposed method the 85 pixels per frame compression level are shown.

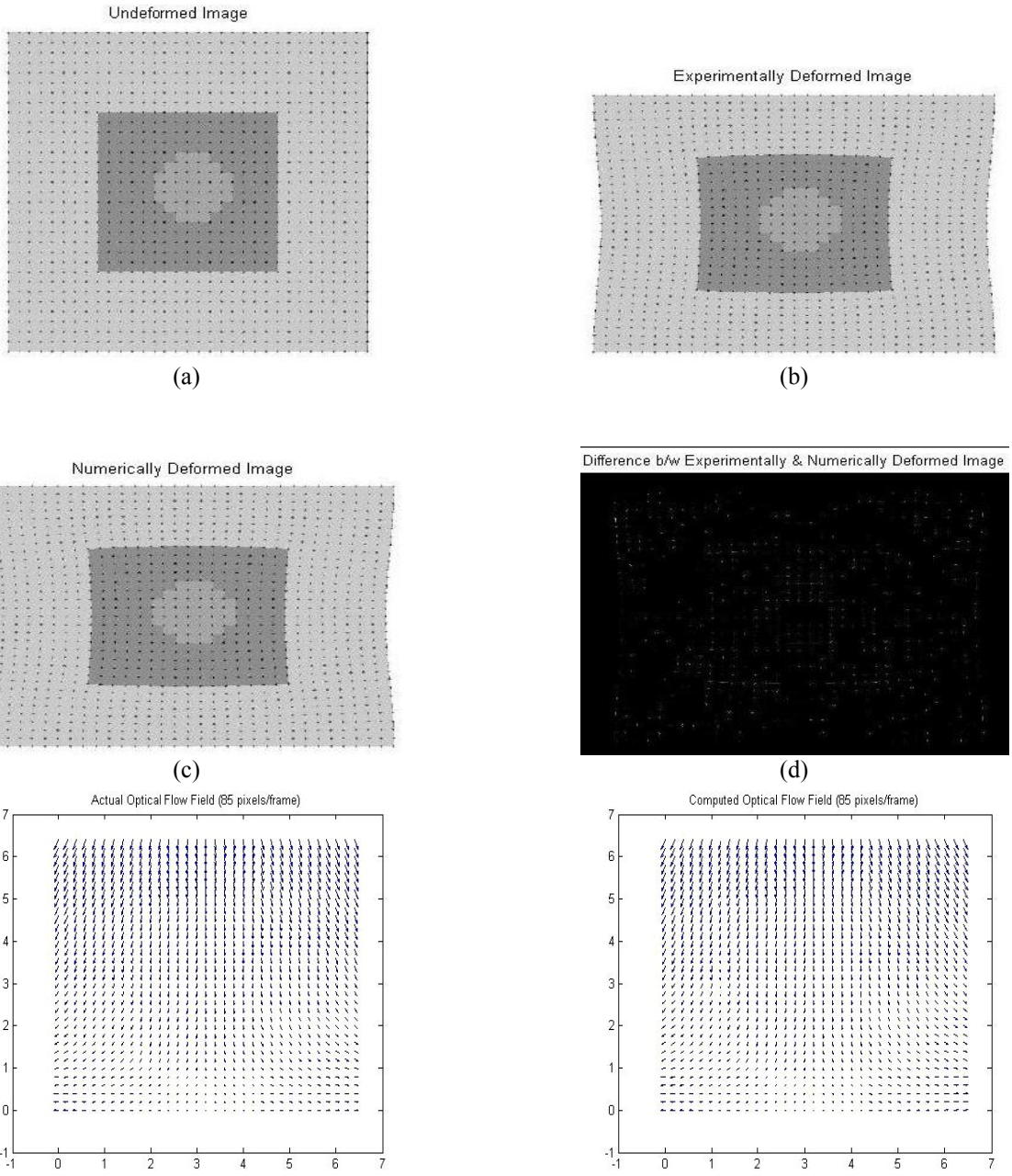

Fig. 7: a) baseline image, b) experimentally deformed image, c) image resulting from applying the proposed method, d) difference between the experimentally deformed and the numerically deformed images e) actual optical flow field and f) computed optical flow field for 85 pixels/frame compression level, respectively.

Fig. 8 shows the baseline image, the deformed image, final numerically deformed image resulting from applying the proposed method, difference between the experimentally deformed and the numerically deformed images, the actual displacement field and the field acquired by the proposed method the 85 pixels per frame compression level.

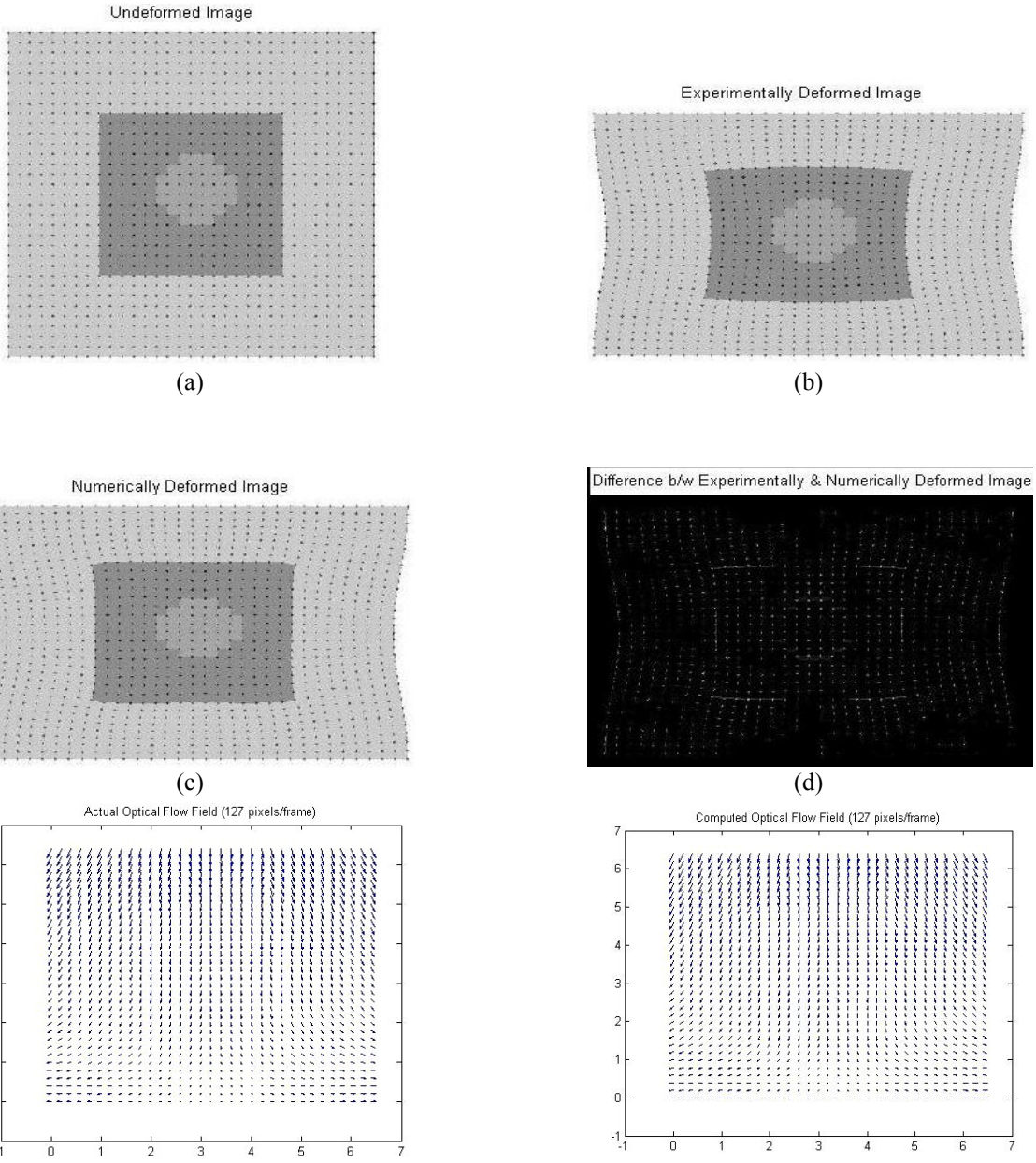

Fig. 8: a) baseline image, b) experimentally deformed image, c) image resulting from applying the proposed method, d) difference between the experimentally deformed and the numerically deformed images e) actual optical flow field and f) computed optical flow field for 127 pixels/frame compression level, respectively.

6. CONCLUSIONS

In this study a novel optical flow technique suitable to determine large deformations was presented. This method was developed to acquire the nodal displacements of soft tissues undergoing mechanical stimulation as applied in hyperelasic elastography. Displacement data acquisition systems requiring magnitude image data are of interest in elastography. While conventional optical flow techniques are capable of acquiring displacements corresponding to small deformation, they lack sufficient accuracy in applications involving large deformations. In this work we used the information

pertaining to tissue mechanical behavior in addition to its geometry before compression and incorporated this information to a hierarchical Horn-Schunck optical flow method. The algorithm is capable of acquiring displacements corresponding to large deformation. The results of applying the proposed method to a numerical phantom undergoing various compression levels (results for 85-pixel and 127-pixel compressions were reported) are promising. The results showed that this approach is capable of calculating the displacement field with high accuracy and the output image of the system is high degree of similarity with the main deformed image.

Future work includes applying this approach to images taken from tissue mimicking phantoms and also using this technique in hyperelastic parameters elastography in which the phantom undergoes large deformations. Accelerating this technique is another objective we will pursue in the future. The aim is to develop a real-time hyperelastic elastography system that can be used in computer aided surgery and needle biopsy.

REFERENCES

[1] Mehrabian H., and Samani A., "An iterative hyperelastic parameters reconstruction for breast cancer assessment", Proc. SPIE, Vol. 6916, 69161C (2008).

[2] Horn B. K. P., "Robot Vision", MIT Press, Cambridge, (1986).

[3] Anandan P., "A computational framework and an algorithm for the measurement of visual motion", International International journal of computer vision [0920-5691], vol:2 iss:3 pg:283, (1989).

[4] Enkelmann W., "Investigations of multigrid algorithms for the estimation of optical flow fields in image sequences," Proc. Workshop Motion: Representation and Control, Kiawah Island, SC, pp. 81-87 (1986).

[5] Horn B. K. P., and Schunck B. G., "Determining Optical Flow," Artificial Intelligence 17:185-203 (1981).

[6] Nagel H. H., "Image sequences--ten (octal) years—from phenomenology towards a theoretical foundation," Proc. 8th Int. Conf. Pattern Recognition, Paris, France (1986).

[7] Barnard S. T., and Thompson W.B., "Disparity analysis of images," IEEE Trans. PAM1 2(4):333-340 (1980).

[8] Glazer F., Reynolds G., and Anandan P., "Scene matching by hierarchical correlation," Proc. IEEE Conf. Comput. Vision and Pattern. Recognition, Annapolis, MD, pp. 432- 441, (1983)

[9] Hildreth E. C., The Measurement of Visual Motion. MIT Press: Cambridge, MA (1984).

[10] Waxman A., and Wohn K., "Contour evaluation, neighborhood deformation, and global image flow: planar surfaces in motion," Univ. of Maryland Tech. Rept. CS-TR- 1394 (1984).

[11] Lucas B. D., and Kanade T., "An iterative image registration technique with an application to stereo vision", in: DARPA Image Understanding Workshop, pp. 121–130 (1981).

[12] Gao L., Parker, K. L., Lerner R. M., and Levinson S. F., "Imaging of the elastic properties of tissue-A review". Ultrasound in Med. & Biol., Vol. 22, No. 8, pp. 959-977 (1996).

[13] Kim J. and Sikora T., "Hybrid Recursive Energy-based Method for Robust Optical Flow on Large Motion Fields" IEEE Int. Conf. on Image Processing (ICIP), Genova, Italy, Sept. (2005).

[14] Black M. J., and Anandan P., "The robust estimation of multiple motions: parametric and piecewise smooth flow fields," Computer Vision and Image Understanding, Vol. 63, No. 1 pp. 75-104 (1996).

[15] Barron J. L., and Khurana M., "Determining optical flow for large motions Using Parametric Models in a Hierarchical Framework," Vision Interface, Kelowna, B.C., pp. 47-56 (1997).

[16] Shannon C. E., "A mathematical theory of communication" Bell Syst. Tech. J. 27 379–423, 623–56,(1948)

[17] Miga M. I., "A new approach to elastography using mutual information and finite elements", Physics in medicine & biology [0031-9155] vol:48 iss:4 pg:467 -80, (2003).

[18] Samani A., and Plewes D. B., "A method to measure the hyperelastic parameters of ex vivo breast tissue samples," Physics in Medicine and Biology, vol. 49, pp. 4395-4405 (2004).